The Meteoritical Society

Meteoritics & Planetary Science 46, Nr 10, 1551–1564 (2011)
doi: 10.1111/j.1945-5100.2011.01248.x

Magnetism and mineralogy of Almahata Sitta polymict ureilite (= asteroid 2008 TC_3): Implications for the ureilite parent body magnetic field

Viktor H. HOFFMANN[1,2*], Rupert HOCHLEITNER[3], Masayuki TORII[4], Minoru FUNAKI[5], Takashi MIKOUCHI[6], Melanie KALIWODA[3], Peter JENNISKENS[7], and Muawia H. SHADDAD[8]

[1]Department of Geo- and Environmental Sciences, University of Muenchen, Theresienstrasse 41, 80333 Muenchen, Germany
[2]Department of Geosciences, University of Tuebingen, Sigwartstrasse 10, 72076 Tuebingen, Germany
[3]Mineralogical State Collection, Theresienstrasse 41, 80333 Muenchen, Germany
[4]Department of Geosphere-Biosphere System Science, Okayama University of Science, 1-1 Ridaicho, Okayama 700-005, Japan
[5]National Institute of Polar Research, 10-3 Midori-cho, Tachikawa/Tokyo 190-8518, Japan
[6]Department of Earth and Planetary Science, University of Tokyo, 7-3-1 Hongo, Bunkyo-ku, Tokyo 113-0033, Japan
[7]Carl Sagan Center, SETI Institute, 189 Bernardo Ave., Mountain View, California 94043, USA
[8]Department of Physics and Astronomy, University of Khartoum, P.O. Box 321, Khartoum 11115, Sudan
[*]Corresponding author. E-mail: hoffmann.viktor@gmx.net

(Received 25 February 2010; revision accepted 29 May 2011)

Abstract–The Almahata Sitta meteorite is the first case of recovered extraterrestrial material originating from an asteroid that was detected in near Earth space shortly before entering and exploding in the high atmosphere. The aims of our project within the 2008 TC_3 consortium were investigating Almahata Sitta's (AS) magnetic signature, phase composition and mineralogy, focussing on the opaque minerals, and gaining new insights into the magnetism of the ureilite parent body (UPB). We report on the general magnetic properties and behavior of Almahata Sitta and try to place the results in context with the existing data set on ureilites and ureilite parent body models. The magnetic signature of AS is dominated by a set of low-Ni kamacites with large grain sizes. Additional contributions come from micron-sized kamacites, suessite, (Cr) troilite, and daubreelite, mainly found in the olivine grains adjacent to carbon-rich veins. Our results show that the paleomagnetic signal is of extraterrestrial origin as can be seen by comparing with laboratory produced magnetic records (IRM). Four types of kamacite (I–IV) have been recognized in the sample. The elemental composition of the ureilite vein metal Kamacite I (particularly Co) clearly differs from the other kamacites (II-IV), which are considered to be indigenous. Element ratios of kamacite I indicate that it was introduced into the UPB by an impactor, supporting the conclusions of Gabriel and Pack (2009).

INTRODUCTION

It is assumed that in the early history of our solar system many small bodies, including planetesimals with diameters as small as 150 km, differentiated to form crust, mantle, and core, and eventually developed an active magnetic dynamo (Rochette et al. 2009b, and references therein). This hypothesis can be tested by investigations of the fragments of asteroid 2008 TC_3. For the first time ever, we have a direct match of asteroid remote sensing observations, an asteroid's collision with Earth, and a witnessed fall of the asteroid's fragments that can be investigated in our laboratories, providing a direct link from an asteroidal meteorite to its parent body.

Asteroid 2008 TC_3 was discovered by the automated Catalina Sky Survey at Mt. Lemmon, Tucson, Arizona, USA, on October 6, 2008, on a collision course with Earth. After entry into Earth atmosphere on October 7, 2008, the small asteroid exploded at about 37 km altitude over the Nubian Desert/Sudan. Meteorite search campaigns led by P. Jenniskens (SETI) and M. Shaddad (University of Khartoum) recovered numerous fragments of the asteroid in the North Sudan desert (Jenniskens

et al. 2009; http://asima.seti.org/2008TC3/; Shaddad et al. 2010). The meteorite was named Almahata Sitta and classified as an anomalous polymict ureilite (Jenniskens et al. 2009, 2010; Zolensky et al. 2010).

Detailed investigations of this extraordinary event are documented in Jenniskens et al. 2009, in this special volume, and at http://asima.seti.org/2008TC3/, focusing on the three main topics (1) observations on 2008 TC_3 by telescopes, remote sensing data, analysis of the orbit, etc.; (2) collision with and transfer through Earth atmosphere and fall; (3) Almahata Sitta meteorite laboratory investigations; and (4) final synthesis of all aspects of the fall. Details of the mineralogy and petrology of Almahata Sitta (AS) can be found elsewhere in the special volume. Jenniskens et al. (2009) classified AS as shock stage 0–1, whereas Mikouchi et al. (2010) proposed S2. In this article, we present the detailed results of investigations of the magnetic signature of two AS fragments (Hoffmann et al. 2009, 2010) and compare the results with data obtained on a few selected ureilites.

Ureilites represent a unique class of achondrites characterized by significant contents of carbon phases such as graphite and diamond, and O-isotopic signatures positioned along the CCAM line. Specific information concerning ureilites and their parent body structure and development, mineralogy, and petrogenesis can be found in Berkley et al. (1980), Downes et al. (2008), Goodrich et al. (1987, 2004, 2007), Goodrich (1992), Mitreikina et al. (1995), Mittlefehldt et al. (2007), Rubin (2006), Singletary and Grove (2003), and Takeda (1989).

Ureilites have rarely been investigated by magnetic methods and detailed or systematic investigations have not been reported. The rare previous investigations have been summarized by Cisowski (1987) and Sugiura and Strangway (1988). Thermomagnetic analysis performed on several ureilites was reported by Rowe et al. (1976). Brecher and Fuhrman (1979) and Nagata (1980a) studied the paleomagnetic signal and paleointensity in terms of likely solar wind magnetic components. Classification of meteorites by magnetic methods was the main purpose of the study by Nagata (1980b). More recently, Rochette et al. (2009a) included a number of ureilites in their magnetic database of achondrites (magnetic susceptibility [MS], χ, and saturation remanence, M_{rs}).

The aims of our current investigations are to examine Almahata Sitta's (paleo-) magnetic signature and magnetic phase composition (focussing on the opaque minerals) to provide new insights into the ureilite parent body magnetism (asteroid 2008 TC_3 belongs to the taxonomic "F" class asteroids according to the reflectance spectrum, Jenniskens et al. 2009, 2010). Herein, we report on the basic magnetic properties of AS, including low-temperature experiments approaching space conditions, and interpretation in terms of likely origin and formation (petrogenesis) of the various magnetic phases (see Hoffmann et al. 2009, 2010). Future publications will focus more on the paleomagnetic signal, meaning, and age constraints.

SAMPLES, METHODS, AND TECHNIQUES

Samples

Two chips of Almahata Sitta ureilite were provided for our pilot study on the magnetic signature by P. Jenniskens (SETI Institute) and M. Shaddad (University of Khartoum) (Fig. 1) (Jenniskens et al. 2010).

1. Chip no. 4 (0.38 g, interior: AS 4), collected December 7, 2008, and chip no. 39 (individual, 1.44 g: AS 39), collected December 30, 2008, both black/dark lithology. Interestingly, some rustiness can be seen on chip no. 39 already, about 3 months after the fall (marked area Fig. 1b).
2. A polished thin section (PTS) was provided by T. Mikouchi (gray lithology) from chip no. 3-1.
3. Two chips of Northwest Africa (NWA) 1241 monomict ureilite (0.31 g) were included in our investigations for comparison (Ikeda 2007) (purchased from E. Haiderer/Vienna).

Polished sections (PS) have been prepared from all samples for optical microscopy and EMPA.

NRM and IRM Experiments

Measurements of Natural Magnetic Remanence (NRM), intensity, and stability (demagnetization in alternating fields [AF]) were carried out using a 2G Cryogenic magnetometer (NIPR), maximum AF field was 100 mT (in *x/y/z* direction). Laboratory Isothermal Magnetic Remanence (IRM) of −300 mT and + 1T fields (in *z*-direction, Pulse Magnetizer MMPM10) and their stability (AF demagnetization, 2G, max. field 100 mT, *x/y/z*) were studied to test for kind and quality of NRM, to exclude or control "magnetic pollution," and to determine the S values after Bloemendal et al. (1992). NRM measurements were performed on the main masses, whereas AF demagnetization and IRM/AF demagnetization experiments were carried out using fragments of both AS4 and AS39 chips.

Magnetic Susceptibility (MS, χ) and AMS

We used kappabridge KLY 3 (NIPR, IFG) and the MFK1-FA (IFG) (both AGICO) for these investigations that were performed at room temperature (RT) on the main masses and fragments. For details concerning

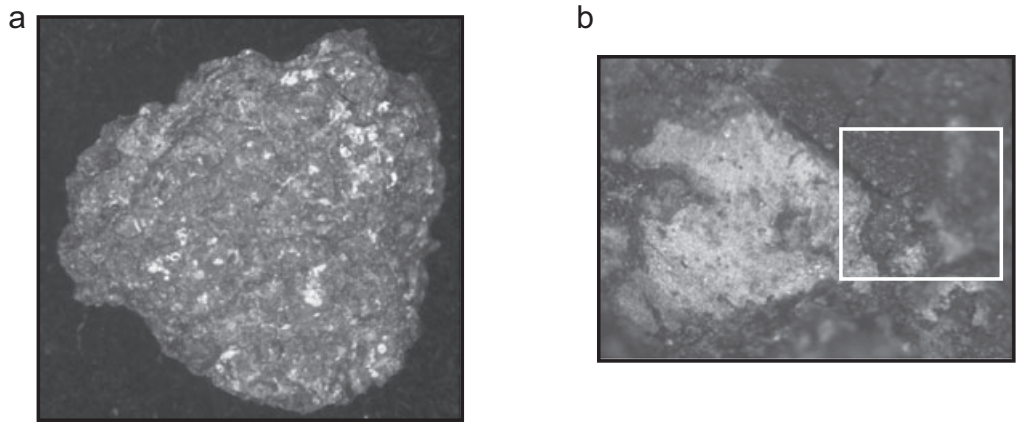

Fig. 1. Optical microscopy of sample AS 39 (stereomicroscope, plane polarized light). a) Sample AS39 individual, size is around 15 mm. b) Large-sized (up to mm size) kamacite sheets (vein material) are typical, some rustiness (terrestrial oxidation) can be recognized in marked area.

Anisotropy of MS (AMS) investigations on stony meteorites, we refer to Gattacceca et al. (2008).

Magnetic Hysteresis, IRM Acquisition, and DC Backfield Demagnetization

Measurements were done on an AGFM 2900 (DG/Tuebingen) at RT. Maximum fields applied were 800 mT in case of hysteresis, and 1T in case of IRM acquisition and DC demagnetization experiments on small fragments.

Low-Temperature IRM Experiments

Measurements were done with an MPMS XL5 at Okayama University of Science applying the following experimental setup (zero-field cooling [ZFC], field cooling [FC]) on small fragments: the sample was first cooled from 300 K to 5 K in zero-field, and then a 1T field was imparted to produce an IRM at 5 K. From 5 K to 300 K, IRM was measured in steps of 1 K (ZFC). Next, the sample was cooled under a 1T field again to 5 K. After switching off the field, IRM was measured up to 300 K in steps of 1 K (FC).

IRM acquisition was done at 300 K from 1 mT to 5T in 100 steps with logarithmically equal spacing. IRMunmix version 2.2 by Heslop et al. (2002) was used for the IRM evaluation.

Thermomagnetic Investigations

Low field (magnetic susceptibility) thermomagnetic runs were performed on KLY3 or MFK1-FA (both Agico). Temperature was 40–800 °C in air, using a fast heating rate to reduce likely alteration effects (i.e., oxidation) in the terrestrial atmosphere.

High field thermomagnetic runs (magnetization [H_{ext} = 0.4T]) were done in air and in Ar, over the temperature range 40–800 °C using a heating rate of 12 °C min^{-1}.

The instrument used was a Natsuhara–Giken (NMB-2000) at Kochi Core Center (KCC), a semihorizontal-type automatic thermomagnetic balance.

The same fragments of both AS chips were used for low-T, IRM, and hysteresis experiments.

Electron Microprobe Analysis

Quantitative chemical data were obtained by electron microprobe analysis (EMPA) using a CAMECA SX100 operated at a 15 keV acceleration voltage and 20 nA beam current (DEG). Synthetic wollastonite (Ca,Si), synthetic NiO, sphalerite (Zn,S), vanadinite (Cl,V), apatite (P), periclase (Mg), corundum (Al), hematite (Fe), escolaite (Cr), natural ilmenite (Mn,Ti), albite (Na), and osumilite (K) were used as standards, and matrix correction was performed by the PAP procedure (Pouchou and Pichoir 1984). The reproducibility of standard analyses was $<1\%$ for each element routinely analyzed. The measurements were performed on a PS of AS 39.

Optical Microscopy

Nikon and Zeiss Axioplan polarization microscopes were used for optical microscopy.

MAGNETIC SIGNATURE AND PHASES

Natural magnetic remanence (NRM) intensities of the two AS samples (main masses) are 15.4 and 2.99×10^{-3} Am^2 kg^{-1}, respectively, data of NRM and

Table 1. Natural magnetic remanence (NRM) and isothermal magnetic remanence (IRM) properties: NRM/IRM record is dominated by soft, low-coercive magnetic phase(s) (high value of S parameter, near −1). For S parameter and REM: see text.

Sample	Mass (mg)	NRM $Am^2\ kg^{-1}$	M_r (−300 mT) $Am^2\ kg^{-1}$	M_{rs} (1T) $Am^2\ kg^{-1}$	S Param.	REM%
AS 4	378	1.54×10^{-2}	n.d.	n.d.	n.d.	n.d.
AS 39	1441	2.99×10^{-3}	n.d.	n.d.	n.d.	n.d.
AS 4 Frags.	2/4	1.71×10^{-2}	1.64×10^{-1}	1.67×10^{-1}	−0.98	10
AS 39 Frags.	4/14	7.79×10^{-3}	1.52×10^{-2}	1.57×10^{-1}	−0.96	5

Note: n.d. = not determined.

IRM experiments are provided in Table 1 and Fig. 2. We also investigated NRM and IRM (as well as other magnetic parameters) on a subsample basis, to check for reliability and homogeneity in terms of intensities and directions. Small fragment NRMs are in the range of the main masses. Log Mrs values (in $10^{-3}Am^2\ kg^{-1}$) are in the range of other ureilite falls (Novo Urei and Haverö) (Rochette et al. 2009a). NRM resembles a typical kamacite-based NRM that can be demagnetized at quite low magnetic fields, but is directionally stable, similar to that seen in earlier ureilite studies (Sugiura and Strangway 1988). The REM values (NRM/IRM) of 10 and 5%, respectively, would point to minor anthropogenic "magnetic pollution" effects from artificial terrestrial magnetic fields. However, it was confirmed by the finders that the samples have been kept away from any magnetic fields in the field and during storage in the laboratory. However, the possibility of exposure of the samples to minor magnetic fields during transportation cannot be completely excluded. Comparison of NRM and IRM behavior during AF demagnetization as shown in Figs. 2a–d excludes significant influence of unwanted magnetic fields and respective magnetic remanences. The S parameter, which provides some indications for the dominant magnetic phase(s) in terms of their remanence coercivity values, is close to one, pointing toward soft magnetic phases such as Fe-Ni metal components as major NRM carriers.

The NRM of AS most probably represents an extraterrestrial magnetic remanence of which the details and the origin, as well as ages, are currently under study and will be reported elsewhere. The NRM is quite strong in intensity, typical for ureilites, and stable in direction, typically known for kamacite-based NRMs, demagnetized already at low fields around 10 mT (Sugiura and Strangway 1988).

In recent years, certain magnetic parameters such as magnetic susceptibility and saturation remanence (M_{rs}) have been proposed for the routine classification of stony meteorites (e.g., Rochette et al. 2009b and references therein: achondrites. The main advantages of the magnetic methods are that they are fully nondestructive, reproducible, repeatable, and applicable in a laboratory, in any museum or other collection, even in the field, and can therefore be used specifically for investigations on very precious materials that are only available in low quantities. In this way, heterogeneities in terms of material properties, such as the concentration and type of magnetic phases, terrestrial alteration effects, or possible misclassifications can be detected (e.g., Hoffmann et al. 2008).

Magnetic susceptibility values (log χ in $10^{-9}\ kg\ m^{-3}$) of the AS main masses were found to be 4.84 and 4.93, whereas small subsamples gave values of 4.92 and 4.98, respectively (Table 2). Magnetic susceptibility values of two investigated NWA 1241 chips were lower (4.68 and 4.79). Rochette et al. (2009a) reported the mean value of three ureilite falls as 4.95, and of all 50 investigated ureilites as 4.39 (please see Table 2 for details). The AS MS values are in good agreement with these earlier findings and also with recent MS data given for Almahata Sitta by Kohout et al. (2010), reflecting the absolute fresh material, whereas the lower values of the finds (NWA 1241) are most probably a result of terrestrial alteration. However, the difference in magnetic mineral composition also has to be taken into account.

We have started to investigate the anisotropy of magnetic susceptibility (AMS) on the AS main masses. Herein, we present our first results, because AMS data have not been reported so far on ureilites, and provide AMS data of HED and Martian meteorites for comparison in Table 3 (Gattacceca et al. 2008). Anisotropy of magnetic susceptibility is an indicator of the degree of shock that a given meteorite has experienced, but is also influenced by, for example, particles/grain shapes. HEDs and Martian meteorites represent magmatic rocks like ureilites, partly breccias, which are generally characterized by low porosities and high densities. This contrasts with the AS samples that we have investigated. We found P values (degree of anisotropy) of 1.315 and 1.531, which are significantly higher than those of HED or Martian meteorites in which the magnetic fabric is most probably impact related.

Magnetic hysteresis, IRM acquisition, and DC backfield demagnetization experiments have been performed on subsamples, small fragments of both main

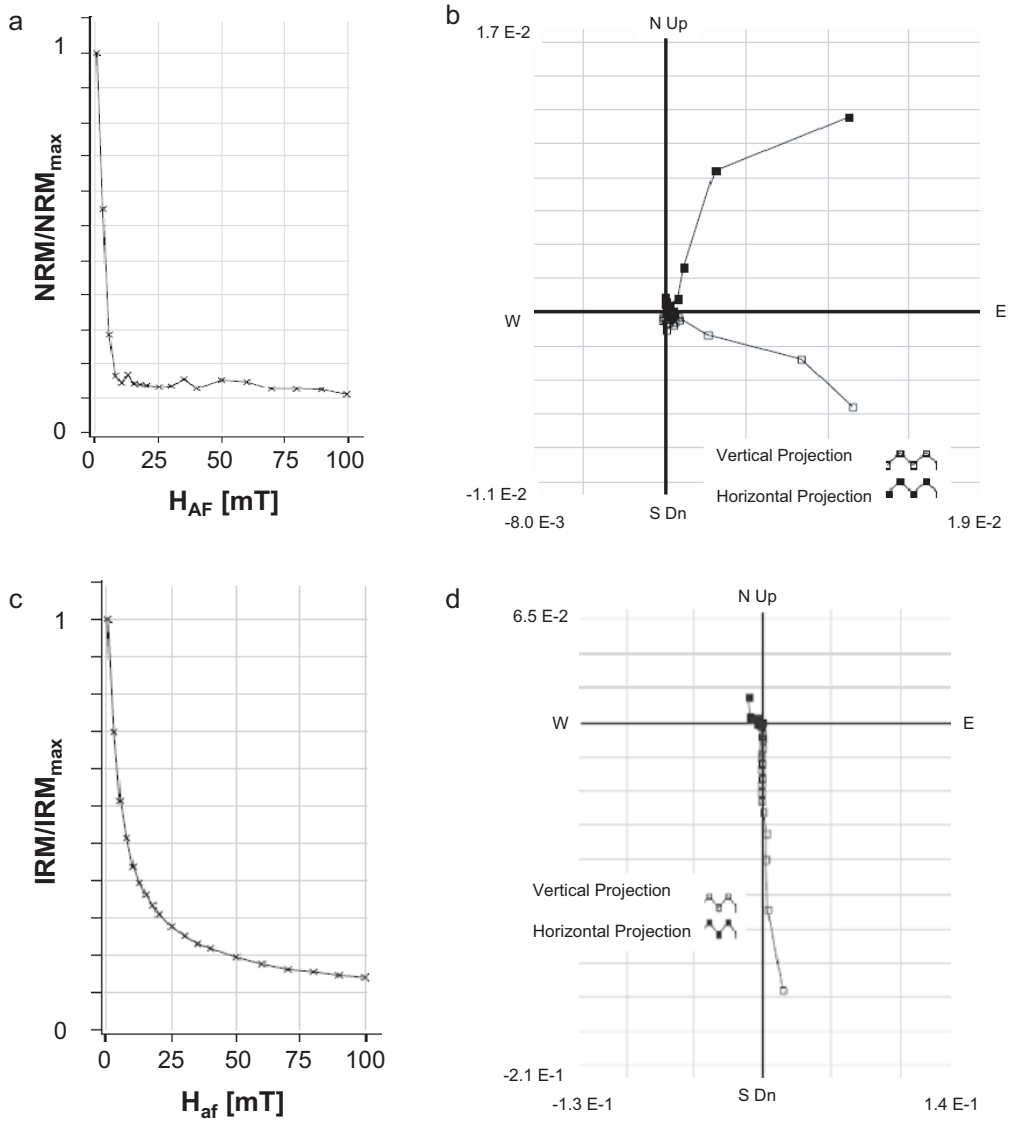

Fig. 2 Alternating field demagnetization of NRM of an AS 4 fragment: a) NRM intensity decay and b) vector diagram. Alternating field demagnetization of a saturation IRM (1T, *z*-direction) of an AS 39 fragment: c) IRM intensity decay and d) vector diagram.

masses. Our hysteresis data show complex magnetization behavior on AS4, indicating strong magnetic interactions, whereas AS39 revealed normal hysteresis curves (see Fig. 3). M_s and M_{rs} values of AS and NWA 1241 are comparable; H_c and H_{cr}, however, are significantly higher in the case of NWA 1241 (16.5 and 24.1 mT for the latter), which points to differences in magnetic phase composition and acting particle sizes (domain state). The further interpretation of the hysteresis results in terms of particle size and shape, and domain state of the magnetic recorders is highly complex: first, most likely, we have a complex mixture of various magnetic phases with incompletely understood magnetic properties, and secondly, strong magnetic interactions acting between at least some of these magnetic phases (Tauxe et al. 1996; Dunlop and Özdemir 1997). Only after a detailed characterization of these phases and after unmixing the various contributions to the hysteresis behavior, it might be possible to interpret the signature correctly, and is the subject of our ongoing investigations. The problem is clearly addressed by the low M_{rs}/M_s values (<0.1) on the one hand which would indicate multidomain (MD) behavior in the case of simple systems, and H_{cr}/H_c values close to or around 1 on the other hand, which would point toward single-domain (SD) like behavior. Extensive and detailed work on the identification and

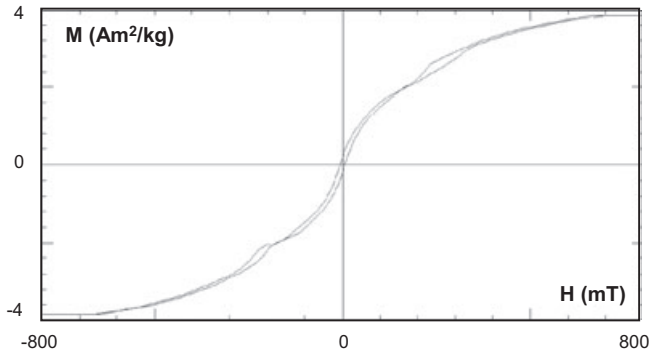

Fig. 3. Hysteresis curve of AS 4 fragment: note the presence of strong magnetic interactions and/or different dominating grain size fractions as indicated by the complex shape of the hysteresis curve.

Table 2. (a) Magnetic susceptibility (χ) data of Almahata Sitta and two NWA 1241 chips. (b) Ureilite MS values as reported by Rochette et al. (2009a).

Sample	Type	Mass (g)	Log χ (in 10–9 $Am^2\ kg^{-1}$)
NWA 1241	Ureilite, monomict	0.318	4.68 ± 0.01
		2.334	4.79 ± 0.01
AS 4	Ureilite, polymict	0.378	4.84 ± 0.01
AS 39	Ureilite, polymict	1.441	4.93 ± 0.01
AS 4-1	Ureilite, polymict	Fragm.	4.92 ± 0.01
AS 39-1	Ureilite, polymict	Fragm.	4.98 ± 0.01

Ureilite MS data by Rochette et al. (2009a):
Three falls (Dyalpur, Haverö, Novo Urei) mean 4.95 ± 0.14; All investigated ureilites (50, without falls) average 4.39 ± 0.31; Lowest MS values (EET83309/pairs, MET01085) mean 3.60; Main factors: Shock and brecciation, terrestrial weathering.

characterization of the magnetic phases is a basic precondition to be able to understand the magnetic signature and record of such complex systems.

As discussed earlier, Rochette et al. (2009b) reported values of magnetic susceptibility and of saturation remanence of a set of ureilites in their database. AS4 and AS39 have log M_{rs} values of 2.29 and 2.20, respectively, (M_{rs} in 10^{-3} $Am^2\ kg^{-1}$), whereas NWA 1241 has a slightly higher M_{rs} of 2.44. In comparison with published data of six ureilites (Goalpara, Haverö, Kenna, Novo Urei, NWA 2703, and NWA 3140) in the range of 2.35–3.13 (mean 2.80), the new data are located at the lower part of the scale, with AS showing even lower values than all previously reported data. Reasons for this behavior are not yet clear because systematic investigations of the magnetic signatures of ureilites that might provide additional constraints are currently not available.

Isothermal magnetic remanence provides information about the remanence coercivity spectrum (H_{cr}) and indirectly about the magnetic phases. Therefore, we conducted additional IRM experiments (full acquisition curve to 5T maximum fields) and statistical unmixing to analyze the IRM spectrum. Figure 4a shows the original IRM acquisition curve (1) and the calculated IRM acquisition curve (2) according to the estimated coercivity spectrum. Figure 4b shows each coercivity spectrum and the sum of four components. Both AS4 and AS39 do not show a perfect agreement between observed and calculated curves. Generally, AS4 and AS39 give very similar results. Our calculations suggest the presence of four magnetic components (phases?) with H_{cr} values of 1.8/2.2 mT, approximately 6.5/8 mT, approximately 43.2/65 mT, and approximately 2284/2243 mT, respectively. The low H_{cr} values (1.8 and 6.5 mT) may point to phases that occur as large multidomain (MD) sized particles (kamacite?), whereas the 43.2/56 mT values could be related to suessite/kamacite in micron-sized particles (SD-PSD state). The highest H_{cr} value could indicate very strong magnetic interactions (exchange coupling) between intergrown or adjacent magnetic phases (daubreelite-troilite-kamacite?).

Low field (magnetic susceptibility) and high field (magnetization, H_{ext} = 0.4T) thermomagnetic runs in air and/or Ar atmosphere allow several magnetic phases to be identified in Almahata Sitta AS4 and 39. Figures 5a and 5b show low field thermomagnetic runs on AS4 and 39. A dominating transition is found at about 770 °C (heating and cooling), indicating low-Ni kamacite; minor transitions around 600 °C and slightly above 400 °C might point to suessite-like phases and eventually schreibersite. Two distinct magnetic phases with Curie temperatures (T_c) of 750–770 °C indicating kamacite with slightly different Ni- or Si contents, and again a suessite-like phase with T_c of 550–600 °C, as well as probably schreibersite with a $T_{c,t}$ around 350–450 °C, point to a more complex mineralogy. At present, we cannot provide a plausible explanation for the nonreversibility of the thermomagnetic behavior. The NWA 1241 thermomagnetic run (Fig. 5c) contrasts significantly with the AS situation. Herein, we find two distinct transitions around 550–580 °C, pointing to suessite with different Si contents, and a minor kink probably suggesting scheibersite. Evidence of kamacite cannot be found in the thermomagnetic run data. Suessite $(Fe,Ni)_3Si$ could be identified for the first time using magnetic methods, and is the subject of our ongoing investigations.

A high-field thermomagnetic curve obtained on fragment AS4 (Fig. 6) reveals basically similar features as seen in Fig. 5a: the curve is dominated by a Curie point at about 770 °C that can be attributed to a Ni-poor kamacite. Additional weak transitions are detected slightly below 600 °C and around 400 °C, which

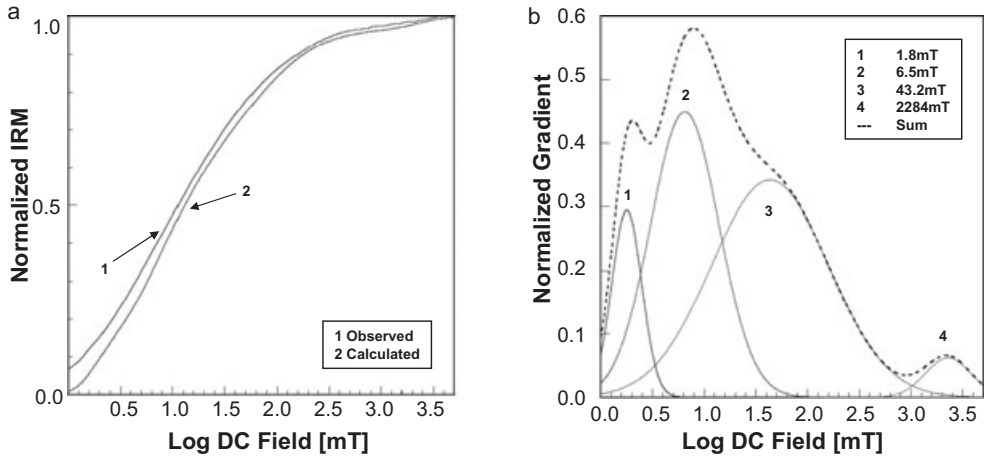

Fig. 4. a) AS4 IRM acquisition curve, b) statistical IRM unmixing of (a).

Table 3. Anisotropy of magnetic susceptibility of Almahata Sitta and two NWA 1241 chips. No other ureilite data are reported, and therefore we provide HED and Martian meteorite data for comparison (mean values, Gattacceca et al. 2008). Magnetic susceptibility (χ) is given in 10^{-9} Am^2 kg^{-1}.

Sample	Type	Mass gr	Log χ	P	T	Fabric
AS 4	U-P	0.378	4.84	1.315	0.146	oblate
AS 39	U-P	1.441	4.93	1.531	−0.159	prolate
NWA 1241	U-M	0.318	4.68	1.267	0.198	oblate
		2.334	4.79	1.289	0.560	oblate
						Comment
Diogenites	HED	n.d.	2.53	1.115	0.110	Mean val.
Eucrites	HED	n.d.	2.62	1.129	0.450	Mean val.
Howardites	HED	n.d.	2.64	1.142	0.233	Mean val.
Nakhlites	Martian	n.d.	2.61	1.023	0.476	Mean val.
Shergottites	Martian	n.d.	2.62	1.059	0.214	Mean val.

Notes: P = degree of anisotropy; T = shape parameter.

basically coincide with the findings in Fig. 5a, most probably suessite and schreibersite. The thermomagnetic results suggest high concentrations of low-Ni kamacite, with slight variations in Ni content, and low to very low concentrations of the other phases. Evidence for taenite cannot be found in our AS samples.

In the low-T regime, additional phases such as Fe-bearing silicates (both olivines and pyroxenes) and specifically Fe-Cr-(Ti) sulfides such as the daubreelite–heideite series or chromite have to be taken into account because they exhibit strong magnetic coupling effects below their Curie or Neel transitional temperatures, and consequently may represent important magnetic recorders. Meteorites can pick up low-temperature magnetic signals during several periods of time within their history, for example, on a daughter body of the parent after collision and/or destruction or during transfer through space. Therefore, to take into account conditions in space, one needs to include the low-temperature regime of the magnetic properties in the laboratory experimental setup to fully control the magnetic signature and recording processes.

We have performed a series of low-temperature experiments of IRM (zero-field cooling and field cooling of a 1T IRM at 5 K), see Fig. 7. No significant features could be found in the low-T regime of IRM. Weak transitions of approximately 150 K and approximately 50–70 K may point to daubreelite-like phases (Kohout et al. 2007). In general, there are two possible ways to explain low-T IRM behavior (Kosterov and Fabian 2008): when the sample is cooled down from 300 K to a very low temperature under a strong magnetic field, a TRM should be overprinted on the sample. Thus, FC is an ordinal low temperature IRM plus TRM. A second mechanism involves magnetic domain structure-related changes during cooling in a magnetic field. So, phenomenologically, FC-ZFC IRM experiments are found to be useful to identify magnetic mineral phases,

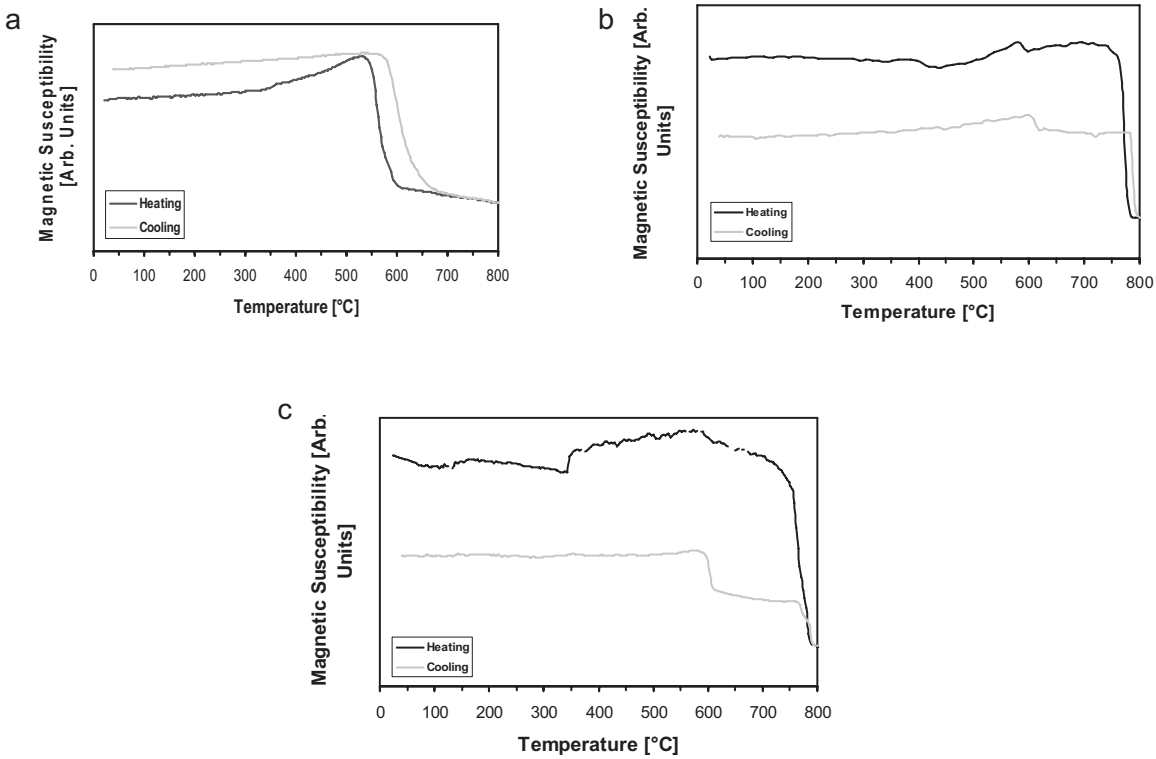

Fig. 5. Low field thermomagnetic curves (MS versus T) as measured in the air. a) NWA 1241, b) AS 4, and c) AS 39.

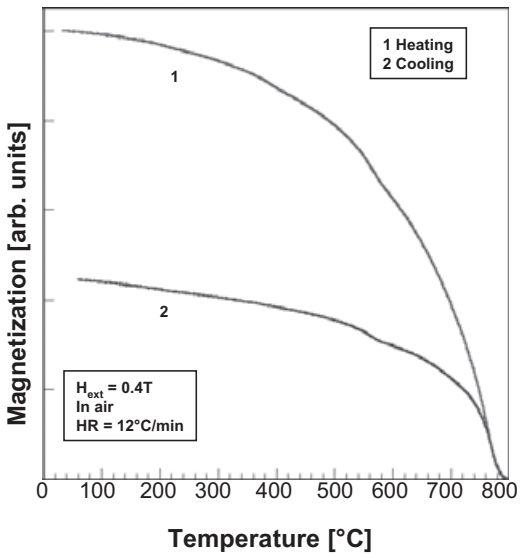

Fig. 6. High field thermomagnetic curve (magnetization) of an AS4 fragment. HR, heating rate.

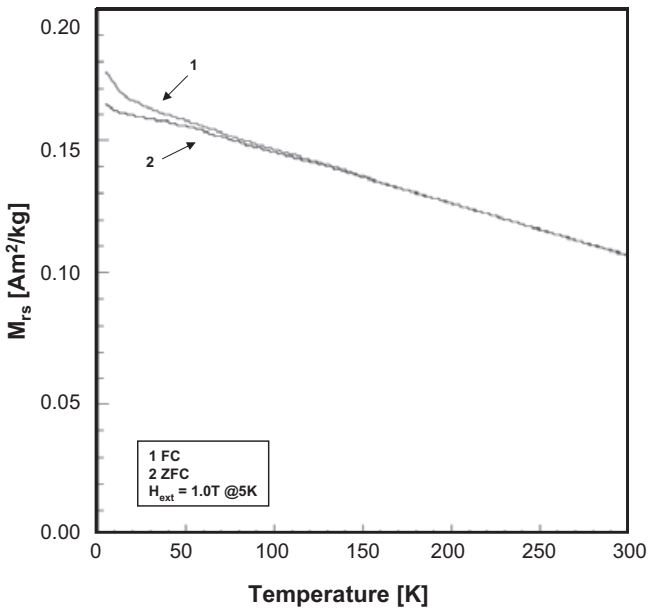

Fig. 7. Low-temperature IRM experiments on an AS 39 fragment. Weak transitions approximately 150 K and approximately 50–70 K could indicate the presence of a daubreelite-like Fe-Cr sulfide.

as well as testing and clarifying recording processes under space conditions.

For these samples, the difference between FC and ZFC is not very significant. Nevertheless, the FC-ZFC shows a rather rapid decrease from 5 to 50 K. This could be unblocking of a TRM component due to the presence of a possible magnetic phase. Daubreelite could be the candidate phase, but there could also be a contribution from a presently unknown magnetic component.

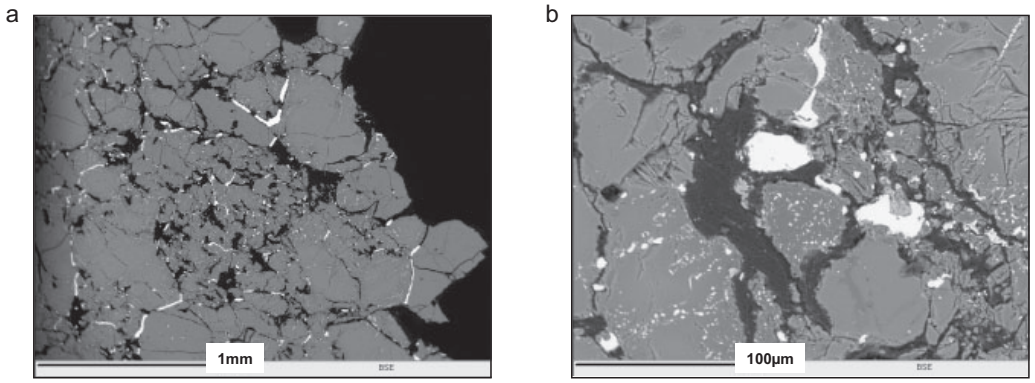

Fig. 8. Backscattered electron SEM images of AS 39 PS. a) Large kamacite laths or sheets can be seen occurring in the vein structures, and many tiny particles of various metal and Fe-sulfide phases in the adjacent silicates. b) Higher magnification view of an area with large kamacites in the veins. High concentrations of micron-sized particles and bleb-shaped opaque (e.g., metals, sulfides) phases are observed mainly in the olivines.

MINERALOGY OF THE OPAQUE MINERALS PHASES IN ALMAHATA SITTA

Figure 8 shows SEM backscatter electron images (BSE) of selected areas in AS39 PS. Large kamacite laths or sheets can be seen in vein-like structures, as well as many tiny (micron-sized) particles of various metal and Fe-sulfide phases in the adjacent silicates. Figure 8b shows a detailed view of an area with larger kamacites in veins surrounded by carbon phases. High concentrations of micron-sized particles and bleb-shaped opaque mineral phases (metals, sulfides, and others such as oxides) are observed mainly in the olivines. Many cracks and fractures represent typical shock features.

Electron microprobe analyses were performed systematically on a large number of mineral phases in an AS39 PS. The main silicate phases are olivine and pyroxene with compositions as reported by Jenniskens et al. (2009) and Zolensky et al. (2010), and the results are summarized in Table 5.

The EMPA investigations on the opaque phases (see Tables 6 and 7, Fig. 9) revealed four distinct kamacite phases with different contents of Fe (between 90.95 and 95.24 wt%), Ni (between 4.31 and 1.22 wt%), and Si (between 3.86 and 0.22 wt%). Chromium (0.18–0.13 wt%) and P (0.37–0.52 wt%) show similar values. Cobalt in significant amounts has only been found in kamacite I (0.20 wt%), whereas Co is near (kamacite IV) or below detection limits in the other kamacites. Kamacite I forms large sheets along grain boundaries between olivines and pyroxenes, whereas the other kamacites form small to very small grains in the carbon-rich fillings between olivine and pyroxene grains. Troilite has significant contents of Cr (1.20 wt%), Si (0.86 wt%), and Mn (0.22 wt%) and a very low-Ni content (0.04 wt%). In addition, a Cr-rich troilite phase with 6.80 wt% Cr and a concomitantly low Fe content (49.25 wt%), and a remarkably high V content (0.39 wt%) has been found. Daubreelite with Cr content of 31.58 wt% has been detected intergrown with troilite. It shows high contents of Mn (2.27 wt%) and V (0.42 wt%). Schreibersite, suessite, or other phases indicated from magnetic experiments could not be identified by EMPA, most likely due to their small particle sizes.

DISCUSSION

Mineralogy

Kamacite

Electron microprobe analysis suggests that there is a compositional distinction between kamacite I and the other kamacite phases. Kamacite I forms large sheets often bordering olivine crystals, thus outlining the olivine crystal shape. This has been used as an argument for the derivation of this kamacite from the adjacent olivine by reduction processes (Goodrich 1992; and references therein). If this hypothesis is correct, it would require a large volume of olivine to be reduced. Given that the fayalite content of olivine is Fa23 at maximum (Zolensky et al. 2010; this study) (Table 5), the formation of such a large volume of kamacite by reduction is problematic. The thickness of the reduced rim on the olivines is between 30 and 50 μm and cannot produce so much kamacite. In addition, kamacite I contains about 0.20 wt% Co, whereas in all other minerals (silicates, metals, and sulfides) Co is near or below detection limit. In addition, the high Ni content of kamacite I (about 4% in average) argues against a formation by reduction of olivine because kamacite formed by reduction of olivine contains very low-Ni contents (Mittlefehldt et al. 1998).

Table 4. Hysteresis properties of the fall Almahata Sitta and the hot desert find NWA 1241.

Sample	Type	M_s Am^2 kg^{-1}	M_{rs} Am^2 kg^{-1}	H_c mT	H_{cr} mT	M_{rs}/M_s	H_{cr}/H_c
AS 4	U-P	3.65	0.226	6.94	7.85	0.06	1.13
AS 39	U-P	1.73	0.162	13.65	10.63	0.09	0.78
NWA 1241	U-M	3.10	0.274	16.48	24.04	0.09	1.46

Notes: M_s = saturation magnetization; M_{rs} = saturation remanence; H_c = coercivity; H_{cr} = remanence coercivity.

Table 5. Chemical compositions of silicates in AS 39 (mean values, wt%).

Pyroxene n = 24		Olivine n = 31	
SiO_2	54.01	SiO_2	38.57
Cr_2O_3	2.52	Cr_2O_3	1.71
Al_2O_3	1.28	Al_2O_3	b.d.
FeO	12.46	FeO	20.56
MgO	b.d.	MgO	41.85
NiO	b.d.	NiO	0.04
Mn	0.44	MnO	0.48
Ca	3.74	CaO	0.37
Total	102.14		103.58
		Fo	0.78

Notes: Fo = Forsterite content of olivine; b.d. = below detection limit.

Table 6. Chemical compositions of metals in AS 39 (wt%). Elements K, Na, Ca, Zn, and Al have been analyzed, but no contents above detection limits have been found.

	Kamacite I n = 27	Kamacite II n = 7	Kamacite III n = 2	Kamacite IV n = 3
Fe	90.95	93.28	94.32	95.70
Ni	4.31	2.21	1.22	2.78
Mn	b.d.	b.d.	b.d.	b.d.
Mg	b.d.	b.d.	b.d.	b.d.
Si	3.86	3.39	3.51	0.22
Cr	0.18	0.15	0.15	0.13
P	0.37	0.43	0.40	0.52
Ti	b.d.	b.d.	b.d.	b.d.
S	b.d.	b.d.	b.d.	b.d.
Co	0.20	b.d.	b.d.	0.07
Total	99.87	99.46	99.60	99.42

Note: b.d. = below detection limit.

Hence, we conclude that kamacite I has a different origin from that of the other metal phases.

The distribution of minor elements between the bulk metal (kamacite) and coexisting sulfides is consistent with known partitioning behavior: Ni, Co, Si, and P are preferentially partitioned into metal, and Cr is preferentially partitioned into sulfides, as is the case with Mn, Ti, and V. The Ni/Co ratio in kamacite I is 21.5, and thus is the range reported for kamacite in chondrites. This is not consistent with the ratios typically found in monomict ureilites that are about 10 (Gabriel and Pack 2009). Similarly, it fails to match the Ni contents and Ni/Co ratios reported by Gabriel and Pack (2009) for presumed equilibrium melting of a UPB. Thus, it strongly suggests that the vein metal in Almahata Sitta polymict ureilite would not have been derived from the UPB, but was introduced by an impactor. More analyses of vein kamacites from different samples and especially from the different lithologies are necessary to constrain the nature of the putative impactor more precisely. Gabriel and Pack (2009) suggested that the "vein metal" (corresponding to our kamacite I) of monomict ureilites was introduced by the impact of an Ni-poor iron meteorite (IIAB or Bellsbank group).

The other kamacites (II, III, IV) have Co concentrations close to or below the detection limits of EMPA, and thus differ clearly from kamacite I. These metals are probably indigenous to the UPB and possibly formed by reduction of Fe-bearing olivines.

Troilite

Troilite is found in small grains in the carbon-rich veins between the olivine and pyroxene individuals and in even smaller grains in the olivines. In the latter occurrence, it shows lines of tiny blebs that seem to follow growth planes (or linear fractures?). Most of the grains are too small to obtain high quality microprobe analysis, but a reduction of coanalyzed olivine material from the mixed analysis allows the identification as troilite. The tiny troilite blebs in the olivines seem to have originated by reduction of the olivine along fractures or other migration conduits as suggested by Berkley et al. (1980). The source of the sulfur remains unclear; however, Berkley et al. (1980) have reported free sulfur from carbon-rich veins in some ureilites.

Chromian Troilite

Troilite phases with up to 6.8 wt% Cr have been identified as small grains in the carbon-rich veins of Almahata Sitta. Chromian troilite has been reported from several ureilites. Troilite from metal-rich clasts in the Dar al Gani 319 polymict ureilite showed chromium contents up to 7.0 wt% (Ikeda et al. 2003), similar to troilites from ALH 82130 (Goodrich 1986; Goodrich et al. 1987). Berkley et al. (1980) reported chromian troilites from Kenna (13 wt%), Haverö (14.1 wt%), Dingo Pup Donga (13.1 wt%), and Dyalpur (8.5 wt%).

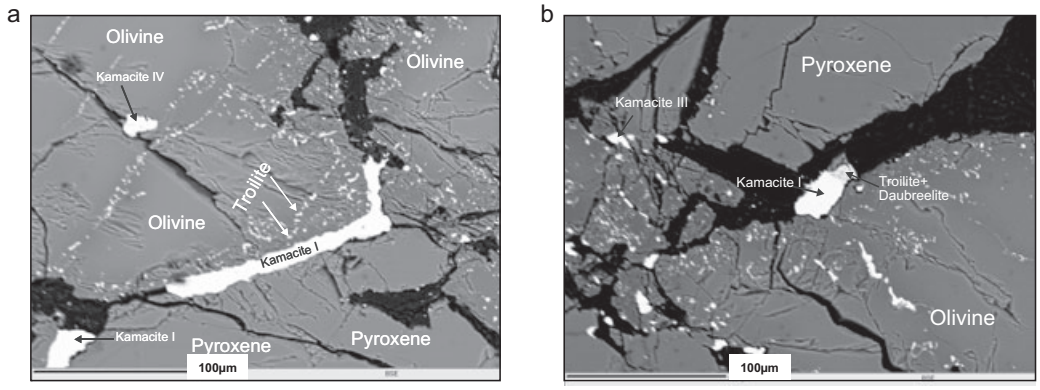

Fig. 9 a, b) Backscattered electron SEM images of a typical region of AS 39. Kamacite I (in veins)/III and IV (in olivine matrix), troilite (in olivine and intergrown with kamacite I) are indicated in typical occurrence. Note the high concentrations of opaque minerals within the olivine grains.

Table 7. Chemical composition of sulfides in AS 39 (wt%). Elements K, Na, Ca, Zn, and Al have been analyzed, but no contents above detection limits have been found.

	Troilite n = 2	Cr- Troilite *n* = 3	Daubreelite *n* = 2	Daubreelite[a] *n* = 8	Daubreelite[b]	Daubreelite[c]
Fe	57.16	49.25	19.40	16.4	22.6	19.38
Ni	0.04	0.04	0.03	b.d.	n.d.	
Mn	0.22	0.64	2.27	2.0	n.d.	
Mg	b.d.	b.d.	b.d.	b.d.	n.d.	
Si	0.86	0.77	0.59	b.d.	n.d.	
Cr	1.20	6.80	31.58	35.4	34.3	36.1
P	0.03	b.d.	0.06	b.d.	n.d.	
Ti	b.d.	0.11	0.11	0.07	0.12	
S	39.93	42.19	46.14	43.4	41.9	44.52
Co	b.d.	b.d.	b.d.	n.d.	n.d.	
V	b.d.	0.39	0.42	n.d.		
Total	99.44	100.19	100.58	97.2	98.92	100

Notes: b.d. = below detection limit; n.d. = not determined.
[a]Neuschwanstein (Hochleitner et al. 2004).
[b]Novo Urei (Goodrich 1992).
[c]Ideal composition.

The authors proposed that the high-Cr sulfides that mainly occur along intergranular veins probably represent indigenous phases.

Daubreelite

Daubreelite is a rare, but not uncommon mineral from ureilites. In Almahata Sitta polymict ureilite, it has been found intergrown with troilite embedded in the carbon-rich veins. It has a high Mn content up to 2.27 wt%, similar to daubreelite from Neuschwanstein EL6 chondrite with 2.0 wt% (Hochleitner et al. 2004). Daubreelites have been reported from ureilites, but mostly without giving a detailed analysis (Goodrich et al. 2004). Especially mentioned are the Haverö ureilite (Mitreikina et al. 1995) and the Kenna ureilite (Farquhar et al. 2000). Berkley et al. (1980) reported analyses of daubreelites from Novo Urei (see also Table 7).

MAGNETIC SIGNATURE

In Alamahata Sitta, we found a variety of magnetic phases including kamacite(s) (low-Ni), troilite, and daubreelite. Schreibersite (most likely) and suessite could only be detected by magnetic methods. The magnetic signature is dominated by two distinct kamacite phases with slightly different Fe/Ni ratios. The role of suessite, schreibersite, or respective intergrowths with other phases such as daubreelite (see hysteresis curve, indicating significant magnetic interactions) needs to be further investigated. Suessite was first found in the North Haig ureilite by Keil et al. (1982) and later confirmed in several other ureilites (Herrin et al. 2007, 2008; Smith et al. 2008; Goodrich et al. 2009). In the case of NWA 1241 (and likely pairs), suessite is the only dominating magnetic phase. However, the knowledge of the

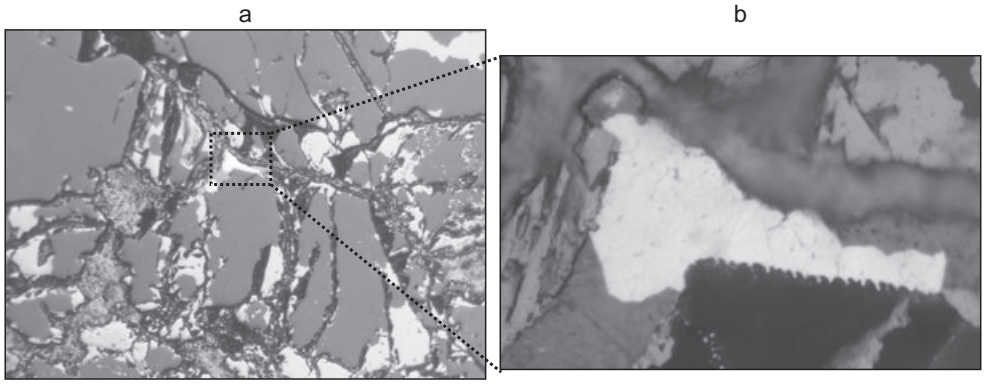

Fig. 10. a) AS39 PS in the optical microscope (plane polarized light), showing typical vein metals (kamacite), graphite, and dominating silicate phases. b) Marked area in higher magnification: the kamacite vein metal penetrates the adjacent pyroxene along the interface. For details see text. Particle size: 50 μm.

magnetic signatures of reduced Fe-Si phases such as suessite is extremely limited at present. Iron-silicide phases such as hapkeite are known from lunar meteorites (Anand et al. 2003). In the past, suessite magnetic properties, e.g., Curie temperatures around 570–600 °C have probably been misinterpreted as magnetite (Rowe et al. 1976). These authors investigated the thermomagnetic properties of a set of ureilites; in the case of Dyalpur, Goalpara, and Haverö, the behavior is dominated by kamacite with Curie temperatures around 750–770 °C; Goalpara shows a weak transition around 500–600 °C, possibly indicating suessite; Novo Urei shows two clear transitions indicating low-Ni kamacite and probably suessite; Dingo Pup Donga and North Haig reveal likely suessite-dominated curves with minor contents of low-Ni kamacite. The latter behavior was interpreted by Rowe et al. (1976) due to magnetite production from a secondary iron-oxide during the experiment. Keil et al. (1982) identified suessite in North Haig, and our experiments on NWA 1241 confirmed that suessite nearly masks a magnetite Curie point, a situation similar to awaruite (which has a Curie point of about 590–610 °C and a low-T transition around 120 K in the range of the Verwey transition of magnetite; Hoffmann et al. 2008).

CONCLUSIONS

It is apparent that the magnetic behavior of AS is very complex and a further interpretation and better understanding requires systematic studies on a subsample basis and on a series of AS chips, taking into account the different known lithologies (Bischoff et al. 2010; Horstmann et al. 2010). It is clear that the paleomagnetic record seems to be dominated by the large kamacite vein metals in significant concentrations. Based on the element composition of the vein metal, most likely this kamacite (I) did not belong to the original ureilite parent body. Consequently, the origin of the kamacite-based paleomagnetic record is probably related to secondary, either impact-related or impactor-related, processes. However, the situation could be different for the other kamacite types and the other detected magnetic phases (suessite, schreibersite, daubreelite, maybe more?) and the individual paleomagnetic record carried by them. A proper separation of these different magnetic records might be only possible by picking and investigating AS chips or fragments after removal of the vein metals as a next and consequent step, and comparing the results with the individual kamacite vein metal paleomagnetic record.

Indigenous or impact have been discussed as possible formation processes for the ureilite vein metal (Gabriel and Pack 2009). Figure 10 shows AS 39 under an optical microscope, revealing typical vein metals (kamacite), graphite, and dominating silicate phases. In higher magnification, it can be seen that the kamacite vein metal penetrates the adjacent pyroxene along the interface, indicating high pressures (impact shock?). This finding supports our suggestion that the vein metal kamacite I is not indigenous, but most likely represents an impactor phase that clearly supports our findings and hypothesis.

The (paleo) magnetic signature of Almahata Sitta is undoubtedly extraterrestrial. However, at present, we are not able to interpret the detailed origin and meaning of the magnetic record and signature, based on the current models for ureilite petrogenesis. The ureilite meteorites are thought to originate from parent bodies that underwent gravitational reagglomeration of possibly several daughter bodies produced by collisional destruction of the original ureilite parent body (e.g., Takeda and Yamaguchi 2008a, 2008b; Herrin et al. 2010). Whether the paleomagnetic record represents magnetization of a primary or secondary ureilite parent body is a topic of our ongoing

investigations. The generally accepted model of the origin of the primary UPB (partially differentiated) suggests a strong relationship between ureilites and CV3 chondrites from oxygen isotope data (Berkley et al. 1980; Holland and Turekian 2003, and references therein). Funaki and Wasilewski (1999) found a magnetic record on Allende (CV3) that suggests an active dynamo field for the CV3 PB; therefore, a similar magnetization process should be expected in the case of the UPB and the ureilite meteorites (Hoffmann et al. 2010).

Acknowledgments—This investigation is part of the Almahata Sitta consortium study (General Info about Almahata Sitta consortium investigations: http://asima.seti.org/2008TC3/) of all aspects of the 2008 TC_3 asteroid collision with Earth and the linked Almahata Sitta ureilite fall. The investigations are supported in part by DFG and University of Tokyo. Our samples have been generously provided by P. Jenniskens (SETI Institute) and M. Shaddad (University of Khartoum). We are very thankful to Y. Yamamoto from Kochi Core Center for measuring and providing the data of the high field thermomagnetic curves (Fig. 6). We highly appreciate the reviews by H. Downes and A. Brearley (AE) as well as of two anonymous reviewers.

Editorial Handling—Dr. Adrian Brearley

REFERENCES

Anand M., Taylor L. A., Nazaraov M. A., Shu J., Mao H. K., and Hemley R. J., 2003. New lunar mineral Hapkeite: Product of impact-induced vapour-phase deposition in the regolith? (abstract # 1818). 34th Lunar and Planetary Science Conference. CD-ROM.

Berkley J. L., Taylor G. J., Keil K., Harlow G. F., and Prinz M. 1980. The nature and origin of ureilites. *Geochimica et Cosmochimica Acta* 44:1569–1597.

Bischoff A., Horstmann M., Pack A., Labenstein M., and Haberer S. 2010. Asteroid 2008 TC_3—Almahata Sitta: A spectacular breccia containing many different ureilitic and chondritic lithologies. *Meteoritics & Planetary Science* 45:1638–1656.

Bloemendal J., King J. W., Hall F. R., and Doh S. J. 1992. Rock magnetism of Late Neogene and Pleistocene deep-sea sediments: Relationship to sediment source, diagenetic processes and sediment lithology. *Journal of Geophysical Research* 97:4361–4375.

Brecher A. and Fuhrman M. 1979. The magnetic effects of brecciation and shock in meteorites: II. The ureilites and evidence for strong nebular magnetic fields. *Moon and Planets* 20:251–264.

Cisowski S. M. 1987. Magnetism of meteorites. In *Geomagnetism*, edited by Jacobs J. A. pp. 525–560.

Downes H., Mittlefehldt D. W., Kita N. T., and Valley J. W. 2008. Evidence from polymict ureilite meteorites for a disrupted and re-accreted singly ureilite parent asteroid gardened by several distinct impactors. *Geochimica et Cosmochimica Acta* 72:4825–4844.

Dunlop D. and Özdemir Ö. 1997. *Rock magnetism: Fundamentals and frontiers*. Cambridge Studies in Magnetism. Cambridge, UK: Cambridge University Press. 573 p.

Farquhar J., Jackson T. L., and Thiemens M. H. 2000. A ^{33}S enrichment in ureilite meteorites: Evidence for a nebular sulfur component. *Geochimica et Cosmochimica Acta* 64:1819–1825.

Funaki M. and Wasilewski P. 1999. A relation of magnetization and sulphidization in the parent body of Allende (CV3) carbonaceous chondrite. *Meteoritics & Planetary Science* 24:A39.

Gabriel A. D. and Pack A., 2009. Ureilite vein metal—indigenous or impact material? (abstract #2462). 40th Lunar and Planetary Science Conference. CD-ROM.

Gattacceca J., Rochette P., Gounelle M., and van Ginneken M. 2008. Magnetic anisotropy of HED and Martian meteorites and implications for the crust of Vesta and Mars. *Earth and Planetary Science Letters* 270:280–289.

Goodrich C.A. 1986. Primary magmatic carbon in ureilites: Evidence from cohenite-bearing metallic spherules. *Geochimica et Cosmochimica Acta* 50:681–691.

Goodrich C. A. 1992. Ureilites—A critical review. *Meteoritics* 27:327–352.

Goodrich C. A., Jones J. H., and Berkley J. L. 1987. Origin and evolution of the ureilite parent magmas: Multi-stage igneous activity on a large parent body. *Geochimica et Cosmochimica Acta* 51:2255–2273.

Goodrich C. A., Scott E. R. D., and Fioretti A. M. 2004. Ureilitic breccias: Clues to the petrologic structure and impact disruption of the ureilite parent asteroid. *Chemie der Erde* 64:283–327.

Goodrich C. A., van Orman J. A., and Wilson L. 2007. Fractional melting and smelting on the ureilite parent body. *Geochimica et Cosmochimica Acta* 71:2876–2895.

Goodrich C. A., Van Orman J. A., Domanik K., and Berkley J. L. 2009. Metal in ureilites: Petrologic characterisation (abstract #1132). 40th Lunar and Planetary Science Conference. CD-ROM.

Herrin J. S., Mittlefehldt D. W., Downes H., and Humayun M. 2007. Diverse metals and sulfides in polymict ureilites EET 83309 and EET 87720 (abstract #2404). 34th Lunar and Planetary Science Conference. CD-ROM.

Herrin J. S., Mittlefehldt D. W., and Jones J. H. 2008. Petrogenesis of Fe,Si-metals in brecciated ureilites (abstract #5327). *Meteoritics & Planetary Science* 42:A109.

Herrin J. S., Ito M., Zolensky M. E., Mittlefehldt D. M., Jenniskens P. M., and Shaddad M. H. 2010. Thermal history and fragmentation of the ureilitic asteroids: Insights from the Almahata Sitta fall (abstract #1095). 41st Lunar and Planetary Science Conference. CD-ROM.

Heslop D., Dekkers M. J., Kruiver P. P., and Van Oorschot I. H. M. 2002. Analysis of isothermal remanent magnetisation acquisition curves using the expectation-maximisation algorithm. *Geophysical Journal International* 148:58–64.

Hochleitner R., Fehr K. T., Simon G., Pohl J., and Schmidbauer E. 2004. Mineralogy and ^{57}Fe Mössbauer spectroscopy of opaque phases of the Neuschwanstein EL6 chondrite. *Meteoritics & Planetary Science* 39:1643–1648.

Hoffmann V., Torii M., and Panaiotu C. 2008. Some new magnetic data on planetary meteorites. *Contributions to Geophysics and Geodesy* 38:35–36.

Hoffmann V., Funaki M., Torii M., Mikouchi T., Hochleitner R., Jenniskens P., and Shaddad M. 2009. Almahata Sitta polymict ureilite: Magnetic signature (abstract). Workshop on Asteroid 2008 TC_3.

Hoffmann V., Hochleitner R., Torii M., Funaki M., and Mikouchi T. Almahata Sitta Consortium, 2010. Magnetism and mineralogy of Almahata Sitta (abstract #2120). 41st Lunar and Planetary Science Conference. CD-ROM.

Holland H. D. and Turekian K. K. 2003. In *Meteorites, comets, and planets*. Treatise on Geochemistry, vol. 1. Elsevier.

Horstmann M., Bischoff A., Pack A., and Laubenstein M. 2010. Almahata Sitta—Fragment MS-CH: Characterization of a new chondrite type. *Meteoritics & Planetary Science* 45:1657–1667.

Ikeda Y. 2007. Petrology of an unusual monomict ureilite, NWA 1241. *Polar Science* 1:45–53.

Ikeda Y., Kita N. T., Morishita Y., and Weisberg M. K. 2003. Primitive Clasts in the Dar al Gani 319 polymict ureilite: precursors of the ureilites. *Antarctic Meteorite Research* 16:105–127.

Jenniskens P. et al. 2009. The impact and recovery of asteroid 2008 TC_3. *Nature* 458: 485–488.

Jenniskens P. et al. 2010. Almahata Sitta (= asteroid 2008 TC_3) and the search for the ureilite parent body. *Meteoritics & Planetary Science* 45:1590–1617.

Keil K., Berkley J. L., and Fuchs L. H. 1982. Suessite (Fe_3Si): A new mineral in the North Haig ureilite. *American Mineralogist* 67:126–131.

Kohout T., Kosterov A., Jackson M., Pesonen L., Kleteschka G., and Lehtinen M. 2007. Daubreelite and troilite as a source of cometary and minor body magnetism in cold environment (abstract #5209). *Meteoritics & Planetary Science* 42:A85.

Kohout T., Jenniskens P., Shaddad M. H., and Haloda J. 2010. Inhomogeneity of asteroid 2008 TC3 (Almahata Sitta meteorites) revealed through magnetic susceptibility measurements. *Meteoritics & Planetary Science* 45:1778–1788.

Kosterov A. and Fabian K. 2008. Twinning control of magnetic properties of multidomain magnetite below—The Verwey transition revealed by measurements on individual particles. *Geophysical Journal International* 174:93–106.

Mikouchi T., Zolensky M., Ohnishi I., Suzuki T., Takeda H., Jenniskens P., and Shaddad M. H. 2010. Electron microscopy of pyroxene in the Almahata Sitta Ureilite. *Meteoritics & Planetary Science* 45:1812–1820.

Mitreikina O. B., Zinovieva N. G., and Granovsky L. B. 1995. Magmatic replacement processes in ureilites. *Antarctic Meteorites* 8:215–224.

Mittlefehldt D. W., McCoy T. J., Goodrich C.A., and Kracher A. 1998. Non-chondritic meteorites from asteroidal bodies. In *Planetary materials*, edited by Papike J. J. Reviews in Mineralogy, vol. 36. Washington, D.C.: Mineralogical Society of America.

Mittlefehldt D. W., Herrin J. S., and Downes H. 2007. Petrology and geochemistry of new ureilites and ureilite genesis (abstract #5280). *Meteoritics & Planetary Science* 42:A109.

Nagata T. 1980a. Paleomagnetism of Antarctic achondrites. *Memoir National Institute Polar Research* 17:233–242.

Nagata T. 1980b. Magnetic classification of Antarctic meteorites. Proceedings, 11th Lunar and Planetary Science Conference. pp. 1789–1799.

Pouchou P. J. and Pichoir F. 1984. A new model for quantitative X-ray microanalysis. *Recherches Aerospatiales* 3:13–38.

Rochette P., Gattacceca J., Bourot-Denise M., Consolmagno G., Folco L., Kohout T., Pesonen L., and Sagnotti L. 2009a. Magnetic classification of stony meteorites: 3. Achondrites. *Meteoritics & Planetary Science* 44:405–427.

Rochette P., Weiss B. P., and Gattacceca J. 2009b. Magnetism of extraterrestrial materials. *Elements* 5/4:223–228.

Rowe M. W., Herndon J. M., and Larson E. E. 1976. Thermomagnetic analysis of meteorites: 4. Ureilites. NASA Report CR-1411-43, N75-146.

Rubin A. E. 2006. Shock, post-shock annealing, and post annealing shock in ureilites. *Meteoritics & Planetary Science* 41:125–133.

Shaddad M. H. et al. 2010. The recovery of asteroid 2008 TC_3. *Meteoritics & Planetary Science* 45:1557–1589.

Singletary S. J. and Grove T. L. 2003. Early petrologic processes on the ureilite parent body. *Meteoritics & Planetary Science* 38:95–108.

Smith C. L., Downes H., and Jones A. P. 2008. Metal and sulphide phases in interstitial veins in "dimict" ureilites—insights into the history and petrogenesis of the ureilite parent body (abstract #1669). 39th Lunar and Planetary Science Conference. CD-ROM.

Sugiura N. and Strangway D. W. 1988. Magnetic studies of meteorites. In *Meteorites and the early solar system*, edited by Kerridge J. F. and Matthews M. S. Tucson, Arizona: The University of Arizona Press. pp. 595–615.

Takeda H. 1989. Mineralogy of coexisting pyroxenes in magnesian ureilites and their formation conditions. *Earth and Planetary Science Letters* 93:181–194.

Takeda H. and Yamaguchi A. 2008a. Two olivine-rich ureilites among nine new Northwest Africa ureilites and their proposed origin (abstract #5187). *Meteoritics & Planetary Science* 43:A.

Takeda H. and Yamaguchi A., 2008b. Contributions of Antarctic ureilites to reconstruction of their parent body and the formation processes with description of three ureilites from Antarctica (abstract #4007). *Meteoritics & Planetary Science* 43:A190.

Tauxe L., Mullender T. A. T., and Pick T. 1996. Potbellies, wasp-waists and superparamagnetism in magnetic hysteresis. *Journal of Geophysical Research* 101:571–583.

Zolensky M. et al. 2010. Mineralogy and petrography of the Almahata Sitta ureilite. *Meteoritics & Planetary Science* 45:1618–1637.